



Optics Letters

Femtosecond laser auto-positioning direct writing of a multicore fiber Bragg grating array for shape sensing

XUNZHOU XIAO,^{1,2} BAIJIE XU,^{1,2} XIZHEN XU,^{1,2} BIN DU,^{1,2} ZIYONG CHEN,^{1,2} CAILING FU,^{1,2}  **CHANGRUI LIAO,^{1,2}**  **JUN HE,^{1,2,*}**  **AND YIPING WANG^{1,2}**

¹Key Laboratory of Optoelectronic Devices and Systems of Ministry of Education/Guangdong Province, College of Physics and Optoelectronic Engineering, Shenzhen University, Shenzhen 518060, China

²Shenzhen Key Laboratory of Photonic Devices and Sensing Systems for Internet of Things, Guangdong and Hong Kong Joint Research Centre for Optical Fibre Sensors, Shenzhen University, Shenzhen 518060, China

*Corresponding author: hejun07@szu.edu.cn

Received 2 December 2021; revised 2 January 2022; accepted 3 January 2022; posted 4 January 2022; published 2 February 2022

A multicore fiber Bragg grating (MC-FBG) array shape sensor is a powerful tool for a variety of applications. However, the efficient fabrication of high-quality MC-FBG arrays remains a problem. Here, we report for the first time, to the best of our knowledge, a new method of directly writing FBG arrays in a seven-core fiber (SCF) through the protective coating using femtosecond laser auto-positioning point-by-point technology, which is accomplished by image recognition and micro-displacement compensation. An MC-FBG array consisting of 140 individual FBGs with a grating length of 2 mm was successfully inscribed into seven cores of a 440 mm-long SCF. Each core contained 20 wavelength-division-multiplexed (WDM) FBGs with wavelengths ranging from 1522.11 nm to 1579.28 nm. In other words, the MC-FBG array consisted of 20 WDM nodes with an interval of 2 cm along the fiber, and each node contained seven identical FBGs integrated in parallel into the fiber cross-section. Moreover, the fabricated MC-FBG array exhibited a strong orientation dependence in bend sensing, with a maximum sensitivity of 55.49 pm/m⁻¹. Subsequently, 2D and 3D shape sensing were demonstrated using the fabricated MC-FBG array, with maximum reconstruction errors per unit length of 4.51% and 10.81%, respectively. Hence, the MC-FBG arrays fabricated using the proposed method are useful in many applications, such as posture monitoring, smart robotics, and minimally invasive surgery. © 2022 Optica Publishing Group

<https://doi.org/10.1364/OL.450274>

Multicore fibers (MCFs) have been rapidly developed due to the tremendous demand for high-capacity data transmission [1], high-precision manipulation [2], and high-performance sensing [3,4]. Bragg gratings inscribed in MCFs, which feature narrowband reflection peaks and a unique fiber geometry, allow novel directional sensing for parameters as curvature [5,6], transverse loading [7], and acceleration [8]. To date, various methods to inscribe fiber Bragg gratings (FBGs) into different types of MCFs have been reported [9–15]. In most reports, FBGs have

been fabricated in all MCF cores using a UV holographic method [9] or a UV phase mask method [10,11]. However, the index modulation induced in each core by these simultaneous exposure methods is uneven due to the lens effect of the fiber, resulting in poor uniformity in these MC-FBGs. Hence, researchers have tried to inscribe an FBG in a specific MCF core by passing a tightly focused laser beam through a phase mask [12,13]. However, it is difficult to precisely adjust the optical setup. Before FBG inscription, the protective coating of the fiber must be removed. Moreover, it is inconvenient to use one phase mask to inscribe a wavelength-division-multiplexed (WDM) MC-FBG array. Recently, a femtosecond (fs) laser point-by-point (PbP) technology for fabricating FBGs in selected MCF cores was reported [14,15]. This method exhibits extraordinary flexibility in the direct writing of serially integrated WDM FBG arrays or parallel-integrated FBG arrays, since the grating pitch and 3D spatial distribution of the FBG can be precisely controlled [16,17]. In addition, these fs laser-inscribed MC-FBGs have excellent high-temperature resistance and hence can be used for sensing in harsh environments. However, rotation of the MCF is required in a conventional fs laser PbP technology to inscribe an FBG in the next core [15]. This procedure is inefficient, especially when inscribing FBGs in a spun MCF. Subsequently, another approach was proposed for fabricating an FBG array in multiple cores of a spun MCF in a single-pass process without fiber rotation [14]. However, MC-FBG arrays fabricated by this method have a fixed grating spacing (i.e., identical to the pitch of the spun MCF) and a short grating length, which leads to broad reflection peaks and is detrimental to achieving a large-scale WDM FBG array.

In this Letter, we propose and demonstrate a new method of fabricating SC-FBG arrays using fs laser auto-positioning PbP technology. Together with a micro-displacement compensation method, an image recognition algorithm [18,19] was used for the real-time alignment of the fs laser-beam focus with the center of each core. Hence, a series of index modulation points (i.e., an FBG) was created in the fiber core by fs laser pulses. Note that no fiber rotation or pre-removal of the coating was required in the inscription process. Then, an SC-FBG array containing 140

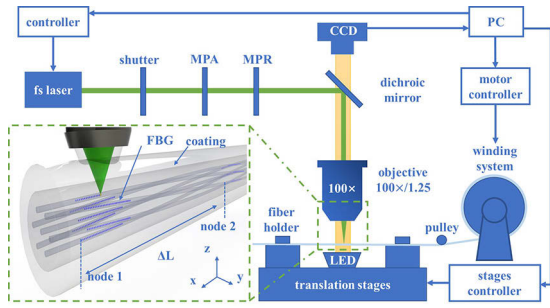


Fig. 1. Experimental setup for inscribing SC-FBGs using a fs laser auto-positioning PbP technology. MPA: motorized power attenuator; MPR: motorized polarization rotator.

FBGs in 20 WDM nodes was created in the wavelength range from 1522.11 nm to 1579.28 nm along a 440-mm-long seven-core fiber (SCF). The bend sensitivities at varying orientations were measured, and a maximum sensitivity of 55.49 pm/m^{-1} was achieved. We further reconstructed the 2D and 3D shapes of the SCF and found that the maximum error per unit length was 4.51% and 10.81%, respectively.

Figure 1 illustrates the setup for fabricating SC-FBG arrays by the fs laser auto-positioning PbP technology. We employed a frequency-doubled regeneratively amplified Yb:KGW fs laser (Pharos from Light Conversion) with a wavelength of 514 nm, a pulse width of 290 fs, and a repetition rate of 200 kHz. A motorized power attenuator and polarization rotator were used to adjust the optical power and polarization of the fs laser beam. A dichroic mirror was used to reflect the laser beam to the objective and transmit the visible illumination beam to the CCD. An oil-immersion objective was used to focus the fs laser beam into the fiber core, and refractive index oil was applied onto the fiber and objective to eliminate the cylindrical lens effect of the fiber. A commercial SCF (YOFC, core diameter: $8 \mu\text{m}$; core spacing: $42 \mu\text{m}$; cladding diameter: $150 \mu\text{m}$) was fixed in place by two fiber holders mounted on a 3D high-precision air-bearing translation stage (Aerotech ABL15010, ANT130LZS, and ANT130V-5) and adjusted to be perpendicular to the incident laser beam. A winding system was used to move the MCF to the preset position. During the SC-FBG inscription, the fs laser beam was fixed and the SCF was moved by the translation stages, and the CCD was used to capture microscope images of the fiber core. Moreover, an image recognition algorithm was used to achieve real-time positioning the center of the fiber core, and a micro-displacement compensation technique was used for auto-aligning the fs laser beam focus with the core center. The fs laser, shutter, fiber holders, translation stages, winding system, and CCD were simultaneously controlled by a computer. Hence, the automatic inscription of SC-FBG arrays was achieved in our experimental setup.

Figure 2(a) shows the process for the auto-positioning of the fiber core by using the image recognition algorithm. First, as shown in Fig. 2(b), the top-view microscope image of the selected fiber core was obtained by the CCD. Then, difference of Gaussians (DOG) filtering was applied to the captured image to increase the contrast of the fiber core and cladding boundaries, effectively eliminating the adverse effects of illumination variation. The average of the grayscale values of the pixels in each row was calculated, yielding a digitalized intensity profile of the fiber cross section along the y axis. As shown in Fig. 2(c),

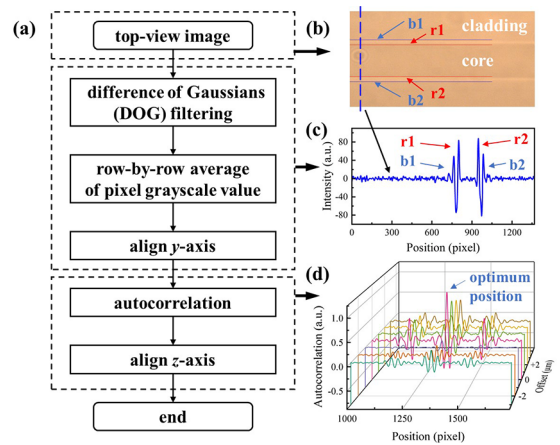


Fig. 2. Auto-positioning of the fiber core center using image recognition. (a) Flowchart of the algorithm; (b) top-view microscope image of a fiber core of the SCF; (c) digitalized intensity profile of a fiber cross-section along the y axis; (d) autocorrelation curves of the digitalized intensity profile of the fiber cross section. As shown in Fig. 2(d), the fiber was scanned vertically along the z axis until the autocorrelation peak reached its maximum, and hence the core center along the z axis was found. As a result, the center of the fiber core was found and aligned to the fs laser beam focus within 16 s.

the upper and lower edges of the fiber core were extracted from the pixel positions of the intensity maximums b_1 , r_1 and b_2 , r_2 , respectively, resulting from the large refractive index differences at fiber core/cladding boundaries. Hence, the fiber core center can be found along the y axis by simply averaging the pixel positions of b_1 , r_1 and b_2 , r_2 . Subsequently, an autocorrelation was calculated for the digitalized intensity profile of the fiber cross section. As shown in Fig. 2(d), the fiber was scanned vertically along the z axis until the autocorrelation peak reached its maximum, and hence the core center along the z axis was found. As a result, the center of the fiber core was found and aligned to the fs laser beam focus within 16 s.

The process for inscribing an SC-FBG array involved three main steps. In step 1, as shown in Fig. 3(a), a single FBG was fabricated in the SCF. First, a section of the coated SCF was fixed

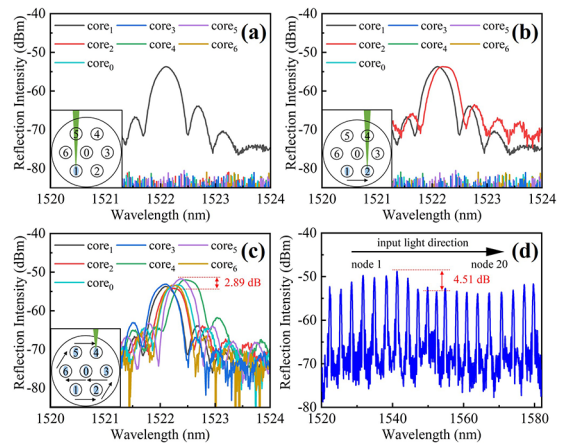


Fig. 3. The process for inscribing a WDM SC-FBG array using the fs laser auto-positioning PbP technology, showing reflection spectra of FBGs fabricated in steps: (a) in step 1, the first FBG was inscribed in SCF core 1 in node 1; (b) and (c) in step 2, the 2nd (upper curve) to the 7th FBGs were sequentially inscribed in SCF cores 2–4 in node 1 (see also Visualization 1); (d) in step 3, a WDM SC-FBG array was inscribed in 20 nodes in the SCF (the WDM FBG array in core 2 is shown here).

in place by fiber holders and the initial position, SCF core 1, was found by moving the translation stage. Then, the fiber core was pre-scanned along the x axis for a distance of 2 mm. During this process, the abovementioned fiber-core auto-positioning method was performed, and the 3D trace for inscribing the FBG was determined. Subsequently, the shutter was opened and the fs laser beam with a pulse energy of 42 nJ was focused into the core center through the fiber coating. Meanwhile, the SCF was translated along the x axis and the laser output was synchronized with the translation stage. In this process, a series of index modulation points with a fixed interval of $1.050\ \mu\text{m}$ were created in core 1 along the designed trace (i.e., the fiber axis). Hence, an FBG with a pitch of $1.050\ \mu\text{m}$ and a grating length of 2 mm was successfully fabricated in SCF core 1.

In step 2, if the inscription of the first FBG was complete, the shutter was closed and the SCF was moved along the y and z axes to find the next core center according to the geometry of the SCF cross section. Then, the shutter was reopened and another FBG was inscribed in the next fiber core. As shown in Figs. 3(b) and 3(c), the fabrication sequence for the SC-FBG proceeded from the bottom up to ensure that no core was obscured; note that the fiber was not rotated. Six other FBGs were sequentially inscribed into cores 2, 3, 0, 6, 5, and 4 of the SCF by repeating step 1 with the same parameters. As a result, seven identical FBGs with almost the same Bragg wavelength were integrated in parallel into the seven cores at the same cross-section in the SCF in 4.2 min (see Visualization 1).

In step 3, if the fabrication of the SC-FBGs in node 1 was complete, the shutter was closed, the fiber holders were loosened, and the SCF was moved to the next position along the fiber (i.e., node 2, which was 2 cm away from node 1) by rotating the fiber spool via a step motor in the fiber winding system. Then, the fiber holders were closed again and the translation stages were moved to a pre-recorded position. A rough profile of the core was observed, and the deviation between the center of the fiber core and the fs laser spot was corrected using the auto-positioning process, as shown in Visualization 1. The SC-FBGs were fabricated in all cores in node 2 by repeating step 2. Note that the SC-FBGs in node 2 had different grating pitches from those in node 1, leading to a different wavelength. Subsequently, the SC-FBGs in the 3rd to 20th nodes were fabricated by repeating this process. As a result, a WDM SC-FBG array consisting of 140 individual FBGs in 20 WDM nodes ranging from 1522.11 nm to 1579.28 nm with an interval of approximately 3 nm was successfully fabricated along a 440 mm-long SCF within 84 min. As shown in Figs. 3(c) and 3(d), the largest difference in peak reflection of the FBGs in node 1 and the FBGs in core 2 was 2.89 dB and 4.51 dB, respectively. This results from the relatively low fs laser pulse energy illuminated on a fiber core (i.e., cores 1 and 2) located at the bottom of the SCF cross section. The reflectivity in these SC-FBGs ranges from 18.90% and 25.61%, which is suitable for wavelength interrogation in subsequent shape-sensing experiments. This fs laser auto-positioning PbP technology is efficient, convenient, and feasible for fabricating SC-FBG arrays.

We studied the vector bend response of the fabricated SC-FBG array via the experimental setup shown in Fig. 4. First, the SCF was spliced with a fan-in/out device (YOFC), which was used to guide the seven cores in the SCF to seven individual single-mode fibers (SMFs). A commercial four-channel FBG interrogator (MOI, SI155) was used to simultaneously interrogate the wavelengths of the FBGs in four cores of the

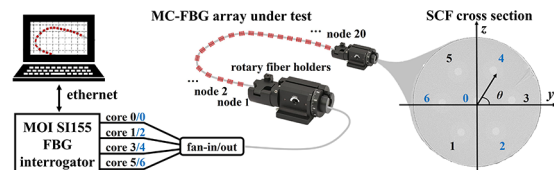


Fig. 4. The experimental setup for testing the vector bend response of the fabricated SC-FBG array.

SCF with a high sampling rate of 5 kS/s and a high wavelength accuracy of 2 pm. Then, the SCF was fixed in place by a pair of rotary fiber holders and mounted on a bend calibration plate, which was engraved with a set of arc grooves with preset curvatures ranging from 5 to $40\ \text{m}^{-1}$. The bend direction was changed by simultaneously rotating the two fiber holders. Note that fiber twisting was avoided during the bend measurements by simultaneously adjusting the two rotary fiber holders. Moreover, the bend orientation angle θ was defined as the included angle between the bending plane and the axis connecting core 3 and core 6 in the SCF. When $\theta = 0^\circ$ or 360° , the SCF was bent along the core 3 to core 6 axis, and core 3 was located on the inner side of the bent SCF. When $\theta = 180^\circ$, the SCF was again bent along the core 3 to core 6 axis, but core 3 was located on the outer side of the bent SCF. The wavelength shifts were recorded for each FBG at varying bend orientations. Due to the limit on the number of interrogator channels, we simultaneously interrogated the FBGs in cores 0, 1, 3, and 5 first, and then switched to simultaneously interrogate the FBGs in cores 0, 2, 4, and 6. The FBG in the central core of the SCF (i.e., core 0) is insensitive to a bend in any direction, and hence could be used to compensate for temperature- or pressure-induced wavelength shifts and to overcome cross-sensitivity to bending and environmental fluctuations in real applications.

Subsequently, we tested the bend sensitivities of the SC-FBGs in different bend directions. The wavelength shift of the FBG in core 6 of node 2 was recorded with different bend direction angles θ from 0° to 360° in steps of 20° , and repeated tests were done under different bend curvatures from 5 to $40\ \text{m}^{-1}$. As shown in Fig. 5(a), all wavelength shifts for a given curvature showed good agreement with sinusoidal curves, i.e., the responses of the wavelength shift to the curvature were different in different bend directions. Then, the bend sensitivities of the FBGs in the six outer cores (i.e., cores 1–6) of node 2 with different bend direction angles θ from 0° to 360° were all measured and drawn in polar coordinates. As shown in Fig. 5(b), there were six perfect ‘8’-shaped patterns corresponding to the six outer-core FBGs, and each ‘8’-shaped pattern included two maxima

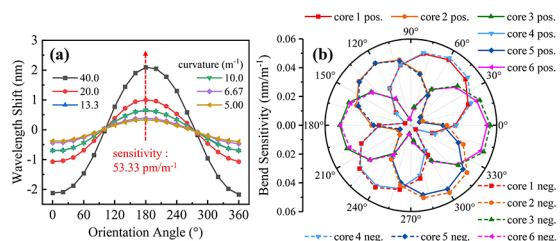


Fig. 5. (a) Measured Bragg wavelength shift of the FBG in core 6 of node 2 as a function of the bend orientation angle θ under different curvatures; (b) bend sensitivities of the FBGs in the six outer cores of the SCF in node 2, plotted for various bend directions in polar coordinates.

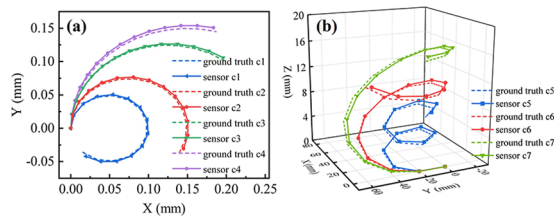


Fig. 6. (a) 2D shape reconstruction of the fabricated SC-FBG array for four different bend radii of 10, 15, 25, and 30 mm; (b) 3D shape reconstruction of the SC-FBG array when wound on three cylinders with diameters of 40, 65, and 80 mm and spiral pitches of 4, 12, and 16 mm, respectively.

and two minima. Maximum sensitivities were achieved when the SCF was bent along the axis connecting this FBG and the center-core FBG, while minimum sensitivities occurred when the SCF was bent in the orthogonal direction. The data were fitted with a linear equation, and the maximum sensitivities of the FBGs in cores 1, 2, 3, 4, 5, and 6 were found to be 52.61, 54.05, 55.49, 55.17, 51.17, and 53.33 pm/m⁻¹, respectively, with corresponding azimuths of 0°, 60°, 120°, 180°, 240°, and 300°. The sensitivity of each FBG fluctuated slightly due to the errors in the rotation angles during the bend test. Moreover, the sensitivities of each pair of FBGs in a diagonal line were almost the same but had opposite signs. Therefore, shape reconstruction can be achieved by using the FBGs in three of the six outer cores and a hexagon geometry in these SCF cores.

Furthermore, 2D and 3D shape reconstruction was achieved using the fabricated SC-FBG array. The orientation and amplitude of the bend vectors at each node of the SCF were calculated from the wavelength shifts of the WDM FBG array in three outer cores (i.e., cores 2, 4, and 6). Frenet–Serret equations were used to reconstruct the 2D and 3D shapes from the bend vectors at each node of the SCF [20]. First, a 2D shape-sensing experiment was carried out. As shown in Fig. 6(a), the reconstructed 2D curves almost coincide with the actual curves for four different bend radii ranging from 10 to 30 mm, and the maximum absolute error in the four tests was 2.98, 1.48, 5.87, and 3.20 mm, which corresponds to a relative error δ_{rel} of 2.37%, 2.21%, 4.51%, and 2.63%, respectively. Note that the formula for the relative error is $\delta_{rel}(s) = |r_{meas}(s) - r_{truth}(s)|/s$, where $r_{meas}(s)$ is the reconstructed curve, $r_{truth}(s)$ is the ground-truth curve, and s is the coordinate along the curve. Then, a 3D shape-sensing experiment was carried out by winding the SC-FBG array on three cylinders with diameters of 40, 65, and 80 mm and spiral pitches of 4, 12, and 16 mm, respectively. As shown in Fig. 6(b), the 3D shapes of the SCF were successfully reconstructed and were in accordance with the real curves. The averaged absolute errors of the three tests were 29.4, 30.3, and 23.5 mm, corresponding to errors per unit length of 10.49%, 10.81%, and 8.42%, respectively. This shape reconstruction error mainly results from the cumulative residual twists; this issue can be resolved by using a pre-twisted MCF [11,14]. Moreover, in comparison with previous works [15], an SCF with a larger core spacing was used and more FBG nodes were integrated, leading to a higher bend sensitivity and a longer sensing distance in the shape sensor demonstrated in this work.

In summary, we have successfully demonstrated a new method of fabricating SC-FBG array shape sensors using a fs laser

auto-positioning PbP technology, which is accomplished by image recognition and micro-displacement compensation. The fabricated SC-FBG array shape sensor consists of 140 FBGs in seven cores and 20 WDM nodes and has a strong bend-direction dependence, with a maximum sensitivity of 55.49 pm/m⁻¹. The SCF shapes were reconstructed in 2D and 3D with a maximum error per unit length of 4.51% and 10.81%, respectively. This approach could provide a promising way to realize a large-scale integrated SC-FBG array intended for high-performance 3D shape sensing in space robotic manipulators, intelligent artificial limbs, and micro-surgical robots.

Funding. National Natural Science Foundation of China (U1913212, 61875128); Guangdong Science and Technology Department (2019TQ05X113, 2019A1515011393, 2019A1515111114); Shenzhen Science and Technology Innovation Program (RCYX20200714114538160, JCYJ20180507182058432, JCYJ20200109114201731).

Disclosures. The authors declare no conflicts of interest.

Data availability. Data underlying the results presented in this paper are not publicly available at this time but may be obtained from the authors upon reasonable request.

REFERENCES

1. D. J. Richardson, J. M. Fini, and L. E. Nelson, *Nat. Photonics* **7**, 354 (2013).
2. G. Anastasiadi, M. Leonard, L. Paterson, and W. Macpherson, *Opt. Express* **26**, 3557 (2018).
3. Z. Zhao, Y. Dang, M. Tang, L. Wang, L. Gan, S. Fu, C. Yang, W. Tong, and C. Lu, *J. Lightwave Technol.* **36**, 5707 (2018).
4. R. Gao and X. Xin, *Opt. Lett.* **44**, 4439 (2019).
5. G. M. H. Flockhart, W. N. MacPherson, J. S. Barton, J. D. C. Jones, L. Zhang, and I. Bennion, *Opt. Lett.* **28**, 387 (2003).
6. D. Zheng, J. Madrigal, H. Chen, D. Barrera, and S. Sales, *Opt. Lett.* **42**, 3710 (2017).
7. M. Silva-López, W. N. MacPherson, C. Li, A. J. Moore, J. S. Barton, J. D. C. Jones, D. H. Zhao, L. Zhang, and I. Bennion, *Appl. Opt.* **44**, 6890 (2005).
8. R. Zhou, F. Chen, S. Li, R. Wang, and X. Qiao, *J. Lightwave Technol.* **39**, 3244 (2021).
9. M. Hou, K. Yang, J. He, X. Xu, S. Ju, K. Guo, and Y. Wang, *Opt. Express* **26**, 23770 (2018).
10. E. Lindley, S.-S. Min, S. Leon-Saval, N. Cvetojevic, J. Lawrence, S. Ellis, and J. Bland-Hawthorn, *Opt. Express* **22**, 31575 (2014).
11. P. S. Westbrook, T. Kremp, K. S. Feder, W. Ko, E. M. Monberg, H. Wu, D. A. Simoff, T. F. Taunay, and R. M. Ortiz, *J. Lightwave Technol.* **35**, 1248 (2017).
12. I. Gasulla, D. Barrera, J. Hervás, and S. Sales, *Sci. Rep.* **7**, 41727 (2017).
13. K. Yang, J. He, C. Liao, Y. Wang, S. Liu, K. Guo, J. Zhou, Z. Li, Z. Tan, and Y. Wang, *J. Lightwave Technol.* **35**, 4670 (2017).
14. A. Wolf, A. Dostovalov, K. Bronnikov, and S. Babin, *Opt. Express* **27**, 13978 (2019).
15. K. Bronnikov, A. Wolf, S. S. Yakushin, A. Dostovalov, and S. Babin, *Opt. Express* **27**, 38421 (2019).
16. X. Liu, Y. Wang, Z. Li, Y. Wang, S. Liu, Y. Wang, C. Fu, C. Liao, Z. Bai, J. He, Z. Li, and L. Shao, *Opt. Lett.* **44**, 5121 (2019).
17. Y. Wang, Z. Li, S. Liu, C. Fu, Z. Li, Z. Zhang, Y. Wang, J. He, Z. Bai, and C. Liao, *J. Lightwave Technol.* **37**, 2185 (2019).
18. A. V. Dostovalov, A. A. Wolf, A. V. Parygin, V. E. Zyubin, and S. A. Babin, *Opt. Express* **24**, 16232 (2016).
19. Y. Yu, J. Shi, F. Han, W. Sun, and X. Feng, *Opt. Express* **28**, 8937 (2020).
20. J. P. Moore and M. D. Rogge, *Opt. Express* **20**, 2967 (2012).